# Size-Dependent Sedimentation Properties of Nanocrystals

**Jennifer A. Jamison, Karl M. Krueger, Cafer T. Yavuz, J. T. Mayo, Denise LeCrone, Jacina J. Redden, and Vicki L. Colvin***

Department of Chemistry, MS-60, 6100 Main Street, Rice University, Houston, Texas 77005



**ABSTRACT** Centrifugation is an increasingly important technique for nanomaterial processing. Here, we examine this process for gold, cadmium selenide, and iron oxide nanocrystals using an analytical ultracentrifuge. Such data provide an accurate measure of the sedimentation coefficients for these materials, and we find that this parameter has a significant dependence on the size and surface coating. Conventional models for particle sedimentation cannot capture the behavior of these nanocrystals unless the density of the nanocrystals is described by a size-dependent term that accounts for both the inorganic core and the organic coating. Using this modification in the particle sedimentation framework, it is possible to estimate sedimentation coefficients from information about the nanocrystal core and surface coating dimensions. Such data are useful in choosing the speeds for a centrifugation process and are particularly important when bimodal nanocrystal distributions are present.

**KEYWORDS:** analytical ultracentrifugation · nanocrystals · iron oxide · cadmium selenide · bimodal sample · polystyrene-coated gold · nanocrystal density calculation

How particles move under the influence of external forces in liquids is a fundamental question which probes the nature of liquids on the nanoscale as well as the interface between nanoparticles and their surrounding fluid.[1] This question also has taken on a practical importance for nanoscience, where nanoparticle movement in response to sedimenting forces is becoming increasingly important for processing. Centrifugation, for example, has been applied for over a decade to improving the size distribution of materials as diverse as quantum dots and single-walled carbon nanotubes.[2–9] More recently, purification of various types of nanoparticle complexes in solution has relied on their different sedimentation properties.[10] In a conventional centrifuge, it is often possible to selectively remove a population of nanoparticles from a mixed sample, or narrow size distributions for a broadly distributed material.

These qualitative applications of centrifugation suggest that a more quantitative picture of the sedimentation process could be of great value. Analytical ultracentrifugation (AU) uses optical tools to evaluate samples during a centrifugation procedure, ultimately providing a direct visualization of the sedimentation of particles. It has emerged as an important tool in characterizing complex macromolecules and their assemblies in both polymer science and biochemistry.[11–23] The extension of this work to polymeric nanoparticles is straightforward, and investigators often use it to evaluate the dispersion and purity of these samples in suspension.[11,24–29] Careful analysis of AU data has been particularly important for determining the densities of spherical polymers using the buoyant density method pioneered by Edelstein and Schachman.[11,12,29,30] AU was historically applied to gold colloids, and more recent examples include nanocrystals of $TiO_2$, $Fe_3O_4$, CdS, $ZrSO_4$, FePt, Pt, ZnO, and various other metal clusters stabilized by micelles or polymers.[31–46] In all of these cases, AU data were employed as a comparative tool, usually with the aim of evaluating particle growth or aggregation under varying conditions. Our group, for example, recently applied AU to examine the formation of bionanoconjugates and to determine the concentration at which gold nanoparticles were saturated with proteins.[47] Despite its increasing use in nanocrystal characterization, quantitative information about the sedimentation properties of nanocrystals is only rarely estimated from AU data sets.

Extracting a sample's average sedimentation coefficient, as well as its distribution, from AU data is possible using several analysis procedures. These parameters are of fundamental interest to nanoscientists, and they also are of practical importance for

*Addressed correspondence to colvin@rice.edu.

Received for review August 3, 2007 and accepted December 28, 2007.

**Published online February 9, 2008.**
10.1021/nn700144m CCC: $40.75

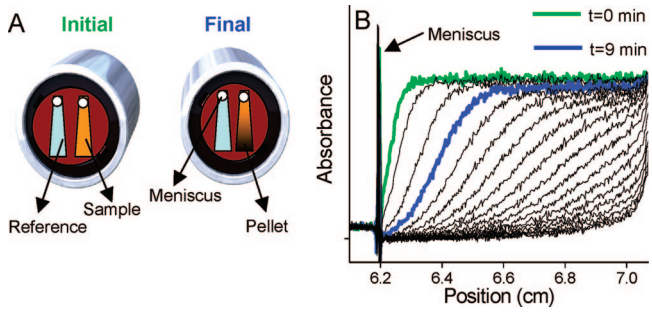


**Figure 1. Overview of the analytical ultracentrifugation process. (A) Prior to sedimentation, the sample is uniformly dispersed in the cell (uniform cell on left). Once the centrifugation process starts, nanocrystals will sediment and ultimately form a pellet in bottom of the cell (non-uniform cell on right). (B) The instrument scans the absorption spectrum of the entire cell from top to bottom during the process; this results in raw data which display at different time intervals the optical density of the sample along the length of the cell.**

nanoparticle separations. If sedimentation coefficients for nanoparticles were known, then ultracentrifuges could be used more efficiently and effectively for separations of closely related populations. Generic models that describe particle movement in a centrifuge can be found in textbooks on colloidal science; they typically balance the centrifugal force that promotes settling against buoyancy, thermal diffusion, and viscous drag.[16,39] Whether these models work for nanocrystals of dimensions under 20 nm is an outstanding question. The sedimentation coefficients predicted by these treatments assume macroscopic models for the solution characteristics. Additionally, for larger particles, the material density is assumed to be a constant value and independent of size; for inorganic nanocrystals, the overall density of the particle will itself be a strong function of size, as the organic coatings will contribute more to the density for smaller systems.[36,39] Thus, nanoscale materials present several features that may require significant modifications to the standard framework for particle sedimentation.

In this work we apply AU to measure the sedimentation coefficients of representative nanocrystals, and we compare these data to conventional models for particle settling. We rely on a variety of nanocrystals, including gold, cadmium selenide, and iron oxide nanocrystals, to demonstrate the generality of our findings. While these materials are generally monodisperse, they do possess size distributions and thus exhibit a spread in their sedimentation coefficients. By varying the size, surface coating, and composition of the materials, we can examine whether models for sedimentation generally need to be modified for the specific case of nanocrystals. In particular, the inclusion of a size-dependent density in these descriptions is essential to describe the observed experimental data; even with this correction, we find that nanoparticle sedimentation depends more steeply on size than predicted. Finally, we show how estimates of the average sedimentation coefficients can permit more effective separation of a nanocrystal sample with a bimodal distribution.

## RESULTS AND DISCUSSION

The empirical sedimentation properties of any material can be captured in a parameter known as the sedimentation coefficient, $s_a$. It can be estimated from raw sedimentation data by evaluating how the boundary demarcating a sedimenting species varies in time. Its form was defined over 80 years ago by Svedberg for a dilute suspension subject to centrifugal force:[48]

$$s_a = \ln\left(\frac{r_b}{r_m}\right)[\omega^2(t_b - t_m)]^{-1} \quad (1)$$

where $\omega$ is the angular velocity and $t_b$ and $t_m$ are the times, in seconds, at positions $r_b$ and $r_m$, respectively. Figure 1A shows a typical configuration for monitoring particle settling *in situ*. Shown in Figure 1B are data collected using an analytical ultracentrifuge which measures the absorption spectra along the cell's length during a sedimentation process. Equation 1 can be applied to the resulting data to estimate a sedimentation coefficient by comparing the position of the sedimentation boundary (50%) at zero time to its position at later times. From such an analysis we find an approximate $s_a$ of 116 Sv (Svedberg units) for 4 nm diameter $Fe_3O_4$ nanocrystals in hexanes. This crude approach to finding sedimentation coefficients in raw data is sufficient for setting the optimal centrifugation speeds for separations of mixtures; however, to extract more quantitative data requires a more complete model of the sedimentation process.

During centrifugation, the sedimentation boundary will broaden both because of the distribution of particle sizes in a sample and because of diffusion. Depending on the heterogeneity of the sample, these two effects can result in shifts of the average $s_a$ estimated with eq 1 to higher values at longer times. To account for diffusion, as well as the presence of many particle sizes, we analyzed our raw data with the van Holde−Weischet (VW) method to extract both an average $s_a$ and a distribution. This model is widely used for biological samples and is well suited for deconvoluting the effects of diffusion and sample heterogeneity on the sedimenting boundary.[40,49] The VW analysis produces a distribution of sedimentation coefficients for every sample which we display here as an integrated frequency distribution (Figure 2). We intentionally chose to display our data as integrated distributions, rather than the more conventional histogram distribution, so as to de-emphasize the wings of the distribution, where the VW analysis can produce scatter. A vertical line in these plots is a sample with only one sedimentation coefficient, while a positively sloped line represents a distribution. Using this analysis pro-

cess, we find that 4 nm diameter $Fe_3O_4$ nanocrystals have an average $s_a$ of 99.1 Sv.

Figure 2 shows the distribution in sedimentation coefficients for model nanocrystal samples of both cadmium selenide and iron oxide; raw data of the type shown in Figure 1 were analyzed using the VW method to provide the integrated frequency distributions. These samples were produced using established techniques, and a variety of characterization tools have confirmed that such systems are non-aggregating and stable suspensions.[50,51] Both materials show increases in their average $s_a$ with increasing diameter as well as nearly vertical integrated frequency distributions. The latter feature corresponds to a very narrow range of sedimentation coefficients. This is consistent with the transmission electron microscopy (TEM) data on these same samples which finds for both materials size distributions typically under 15% (see Supporting Information, Figures S2–S8 and Supplementary Table 1). Because the sample sizes are so uniform, the sedimentation coefficients measured using the VW analysis have a very narrow distribution.

Nanocrystals that have larger core sizes have larger average sedimentation coefficients; this size dependence is not surprising, given the anticipated relationship of the sedimentation coefficient to particle parameters such as radius and density. For spherical particles in dilute suspensions, textbook models for general sedimentation in the absence of centrifugal force predict that

$$s_a = \frac{2R_H^2(\rho_{particle} - \rho_{solvent})}{9\eta} g \qquad (2)$$

where $R_H$ is the hydrodynamic radius of the particle, ρ is the density, η is the viscosity of the solvent, and $g$ is the gravitational constant.[1] To a first approximation, the sedimentation coefficient should scale with the square dimensions of the particle, a prediction in qualitative agreement with the data shown in Figure 2. In addition, the cadmium selenide nanocrystals have lower sedimentation coefficients than the nanocrystalline iron oxides. This is largely a reflection of the different sizes. However, the densities of the nanocrystals also are an important factor for determining their sedimentation coefficients. Even though the densities of bulk cadmium selenide (5.81 g/cm$^3$) and iron oxide (5.17 g/cm$^3$) are comparable, in nanocrystal form these densities are a substantial overestimate. The contribution of the low-density organic coatings are non-negligible in this size range and must be taken into account in order to describe the data.[31,36,39]

To evaluate the importance of these size-dependent effects, we compare in Figure 3 the measured sedimentation coefficients for these model nanocrystals to predictions from eq 2. In order to

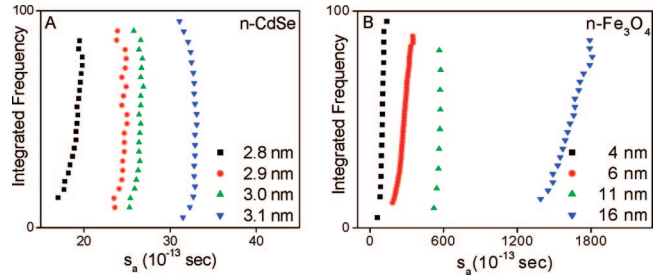


**Figure 2. Size-dependent sedimentation of inorganic nanocrystals. (A) The sedimentation coefficient distributions, displayed as integrated frequency distributions, for four samples of nanocrystalline CdSe in toluene ranging in size from 2.8 to 3.1 nm in core diameter (see Supporting Information, Figures S5−S8). These samples yielded average *s*-values of 21.12, 24.34, 27.76, and 33.00 Sv that corresponded well with TEM core measurements. All samples were run at the same speed and temperature. (B) Sedimentation coefficient distributions for magnetite nanocrystals in hexanes. Core diameters of 4, 6, 11, and 16 nm particles yielded *s*-values of 99.05, 276.5, 567.8, and 1637 Sv, respectively. The samples were run at different speeds to accommodate the drastically different sedimentation rates.**

place data collected in different solvents on the same relative scale, it is necessary to apply a linear conversion factor to the raw data. Using eq 2, this is a straightforward process that provides the equivalent sedimentation coefficients in toluene for samples run in another solvent:

$$s_v(\text{toluene, 20 °C}) = s_a \frac{\eta(\text{solvent})}{\eta(\text{toluene})} \frac{\Delta\rho_{toluene}}{\Delta\rho_{solvent}} \qquad (3)$$

For these data, iron oxide nanocrystal sedimentation coefficients in hexanes are 1.75 times larger than their expected values in toluene at the same temperature.

Figure 3 shows that the size-dependent sedimentation coefficients qualitatively behave as eq 2 would predict, but that the assumption of a constant nanoparticle density vastly overestimates the measured sedimentation coefficients. The solid lines in these figures represent the predictions of eq 2 assuming a bulk density for the particles; the experimental data, espe-

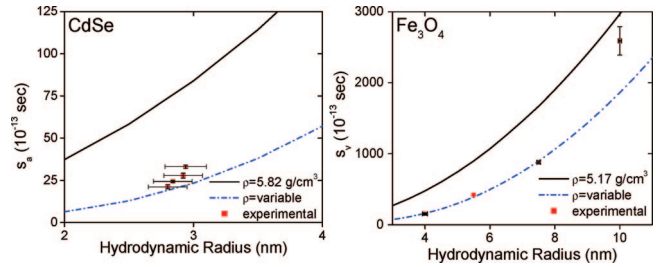


**Figure 3. Size-dependent sedimentation coefficients plotted against nanocrystal size. Hydrodynamic radii take into account nanocrystal density correction using eq 4. We assume a bulk density of 5.17 g/cm$^3$ for magnetite and expect that the largest iron oxide value could be off because of non-stoichiometric Fe/O ratios that occur for large sizes. The black curves in each figure estimate the *s*-values by using bulk density values. The blue curves estimate *s*-values by assuming that the density of particles is size-dependent. (Left) CdSe in toluene (unscaled *s*-values). (Right) $Fe_3O_4$ in hexanes (*s*-values scaled to toluene). Experimental data error bars for hydrodynamic radius are smaller than the data points for particles with core diameters of 4 and 11 nm.**

cially at smaller sizes, are in poor agreement. While lower overall particle densities can provide better agreement, they fail to match the pronounced size dependence in the average sedimentation coefficients. This is because nanoparticle density is not constant with size but varies substantially as relative contributions of the inorganic core and surface coating change with core diameter.

To evaluate whether this size-dependent density could better account for our data, we derived the anticipated density of a nanocrystal consisting of a spherical inorganic core and a thin organic shell. The net density of this nanocrystal-coating assembly can be found *via*

$$\rho_{\text{particle}} = \rho_{\text{shell}} + \left(\frac{(R_H - t)^3}{R_H{}^3}\right)(\rho_{\text{core}} - \rho_{\text{shell}}) \qquad (4)$$

where $t$ is the thickness of the organic shell, $\rho_{\text{shell}}$ is the density of the shell, $\rho_{\text{core}}$ is the density of the bulk inorganic, and $R_H$ ($R + t$) is the hydrodynamic radius. Of these data, the density and thickness of the shell are the most difficult to estimate. We assumed that the organic surface ligands were in a fully extended conformation, yielding a surface coating thickness of 1.4 nm for CdSe and 2.0 nm for $Fe_3O_4$. The actual values could be shorter because of surface packing and interactions between capping ligands.[50] For the organic coating density, we considered a range of densities for polymers (from 1.0 to 1.6 g/cm$^3$) (Supporting Information, Figure S1). In contrast to the shell thickness, where small changes in the values assumed yielded substantial changes in the data, we found that the organic coating density had only a small effect on our predicted nanoparticle densities.

Equation 4 thus provides an estimate of nanoparticle density which, when combined with eq 2, yields a prediction for the sedimentation coefficient *versus* size. We find that, by including a size-dependent density term, even from our simple model, we are able to match quite well the experimental data with a model that has no adjustable parameters (Figure 3, dashed line). Across a range of sizes and materials, the core–shell model captures the absolute values of the experimental data as well as the steep size-dependent sedimentation coefficient measured in both nanocrystal systems. The model could be improved by a more accurate accounting of the non-uniformity of surface coatings, immobilized solvent molecules at the surface or within the coating, and shape effects. Further studies will evaluate these effects in more detail. Note that, for the small particles of interest in this work, dynamic light scattering is not suitable for measuring $R_H$; we thus estimated this parameter by adding the shell thickness to the measured core radius from TEM.

Equations 2 and 4 suggest that nanoparticle density, and ultimately sedimentation properties, can also

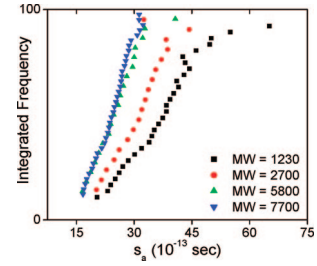


**Figure 4. Sedimentation of polystyrene-coated gold nanocrystals in toluene. The longer the polymer chain, the smaller the density of the particles and the smaller the sedimentation coefficient. Average sedimentation coefficients, from left to right, are 23.00, 23.85, 29.18, and 36.59 Sv, respectively, for polymers of decreasing molecular weight.**

be manipulated through changes in surface coatings. Figure 4 shows the effects of varying the thickness of a surface coating on the sedimentation of gold nanocrystals. In this case, very small gold nanocrystals (core diameter = 2.2 ± 0.2 nm) were coated with polystyrene chains *via* a thiol end group (see Supporting Information, Figure S9). Using eq 2, and a modified density as predicted by eq 4, we estimate that gold coated with a short polymer chain ($M_w$ = 1100) should have $s_a$ = 45 Sv, and the measured value is 37 Sv. A major challenge in analyzing these data is the estimate of the polymer coating thickness; if the polymers are more extended, for example, we find $s_a$ = 39 Sv. A thicker organic coating reduces the average sedimentation coefficient; this is because it lowers nanocrystal−polymer densities for the higher molecular weight coatings. These data illustrate that the sedimentation coefficients of nanocrystals are exquisitely sensitive to the thickness of their surface coatings. Evaluating these surface features directly in solution is challenging yet often critical in understanding nanocrystal properties in biological and environmental settings.

Taken together, the data in Figures 3 and 4 demonstrate that nanocrystal sedimentation properties are strongly dependent on the size and surface. We can estimate, at least semi-quantitatively, the value of their sedimentation coefficients if the nanocrystal density is corrected to include the contribution of the surface coating. As a consequence, nanocrystals display sedimentation coefficients that depend more steeply on their size than conventional particle settling models that predict a scaling of radius squared. This size dependence can be captured by a simple core–shell model for the inorganic core and organic coatings (Figure 3). At large enough sizes, nanocrystal-coating particles will approach the bulk inorganic density and show conventional particle behavior. The exact size where this occurs depends on the coating thickness; however, for standard organic coatings that are 1 nm in thickness, nanocrystals will typically reach about 85% of the bulk density with cores of 35 nm diameter.

While the standard model modified with a size-dependent density is in good semi-quantitative agree-

ment with our experimental data, a more precise comparison would require an independent measure of nanocrystal density. Centrifugation can be applied to this problem for other systems, and indeed sedimentation equilibrium as opposed to sedimentation velocity experiments have been applied to measuring the density of polymers and biomolecules.[11,12,30,52] Unfortunately, these studies require that the solvent density be close to that of the nanoparticle, a constraint that makes it impossible to evaluate higher density ($\rho > 3$ g/cm$^3$) inorganic particles. We attempted to extract nanoparticle density using sedimentation velocity data sets by varying the solvent density and sample temperature. As is apparent in eq 3, a measure of the sensitivity of the sedimentation coefficients to such variables could, in principle, yield the nanoparticle density. However, our observed changes in sedimentation coefficients were equal to our experimental errors over the range of solvent compositions and temperatures that preserved isolated and nonaggregating particles. Future work will focus on more precise measures of sedimentation velocities as well as developing ways to measure nanocrystal density that do not rely on sedimentation.

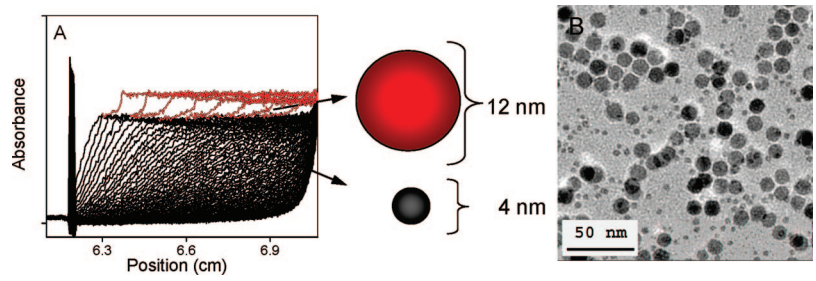


**Figure 5. Bimodal magnetite nanocrystals sample run in hexanes. (A) The raw data (speed optimized for smaller nanocrystals) show two boundary regions, which is indicative of at least two species. (B) TEM image of the sample. More detailed sizing of this sample can be found in the Supporting Information (Figure S10).**

One application for estimating size-dependent nanocrystal sedimentation coefficients is the development of ways to achieve more robust separation of nanocrystal mixtures. Ultracentrifugation is now widely used to purify nanomaterial samples, but rarely do researchers use quantitative information about the sedimentation characteristics of the components. Such information is necessary to select the optimal speed for a process. For separations, it is best to choose the slowest speed so that the faster-sedimenting material deposits completely in a reasonable time frame. If speeds are faster than this optimal value, then more of the smaller material will be removed than is necessary in the pellet. If speeds are too slow, then the larger material will not be removed completely.

Good estimates of nanocrystal sedimentation coefficients can provide information to help choose centrifugation speeds for separating nanoparticle populations. Generally, TEM or other imaging tools can provide dimensions of the inorganic components of various populations in a starting material (Figure 5). With such information about the cores and good estimates of the coating thickness and composition, eqs 2 and 4 can be used to predict the sedimentation coefficients of the individual components. The optimal speed can then be found from eq 1 with a few assumptions about the experiment:

$$\omega^* = \sqrt{\frac{\ln\left(\frac{\text{position}_{\text{end}}}{\text{position}_{\text{start}}}\right)}{ts_a}} \times 9.55 \qquad (5)$$

where $t$ is the time in seconds of the separation experiment, $s_a$ is the sedimentation coefficient in inverse seconds (1 Sv $= 10^{-13}$ s), $\omega^*$ is the speed in revolutions per minute (rpm), and the start position is typically the top of the sample meniscus and the end position would be the bottom of the cell. In most cases, an experiment time of 2 h is short enough to ensure little diffusive spreading of the boundary but long enough to make the start-up and brake time a minor contribution to the run. If we apply eq 5 to a typical sample ($s_a = 100$), with a 1.2 cm fully filled sample cell, then we find an optimal speed of approximately 13 000 rpm.

To illustrate how to use this information in an experimental setting, we prepared a nanocrystal mixture by mixing 4 and 12 nm iron oxide nanocrystals in an approximately 3:2 ratio (see TEM image, Figure 5B, and Supporting Information, Figure S10). This sample simulates the common situation where small nanocrystals must be removed from a larger sample of interest. Because of the vastly different sedimentation profiles of the two particle types, it is possible to physically separate the components within the AU. Application of eqs 2 and 4 for these samples predicts that the two species will have sedimentation coefficients in hexanes of 100 and 700, respectively. In order to sediment out the larger of the two fractions in 0.5 h, we found an optimal speed of ~10 000 rpm. Because we were applying AU, we chose a slightly slower speed so as to have enough sedimentation curves from the larger component for reasonable data analysis. The data clearly show the independent sedimentation of the larger nanoparticles (Figure 5, red lines) from the smaller materials (Figure 5, black lines). Figure 6 shows the resulting distributions of the sedimentation coefficients found from an analysis of the sedimenting species; both fractions of particles are detected, and their sedimentation values are in good agreement with those found in the individual experiments.

These data also highlight the limitations in using AU under single-speed conditions for simultaneously evaluating populations that are widely disparate in size. In general, the time scales of AU experiments should

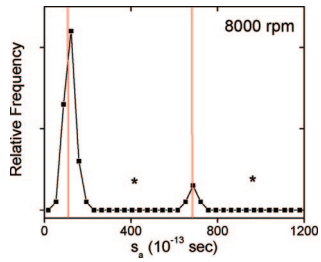


**Figure 6. Sedimentation coefficient distributions for bimodal magnetite nanocrystals. The core diameters of the particles, 4 and 12 nm, yielded $s_a$ values of approximately 100 and 700 Sv, respectively. The red lines denote $s_a$ values of the samples run individually. The analysis process can lead to artifacts when two *s*-coefficients are extracted; these were removed from thes data and their locations denoted with asterisks at 400 and 900 Sv.**

be between 60 and 300 min so as to allow for enough scans to be collected while at the same time minimizing diffusion. Thus, AU at a single speed is best applied to mixtures in which the component sedimentation coefficients do not vary by more than a factor of 5. If ultracentrifugation alone is employed simply to separate materials, there are no such limitations. The best results would be achieved when the *s*-values are substantially different, assuming that the speeds are chosen (eq 5) such that the full sedimentation of one species occurs with only minimal movement of the other. Alternatively, there are established methods to overcome single-speed limitations, such as using turbity optics and/or the gravitational sweep method after running at multiple speeds.[53]

## CONCLUSIONS

Uniform nanocrystals exhibit sedimentation behavior that qualitatively follows the trends predicted for micrometer-sized particles: larger and more dense particles sediment faster in a centrifuge. However, when core diameters are below 20 nm, the sedimentation coefficients depend on nanocrystal size in a way not well described by conventional models because the low-density coating contributes substantially to the overall particle density. Accounting for this size-dependent density provides predictions of nanocrystal sedimentation coefficients that are in good agreement with experimental data. By predicting sedimentation rates, separation of closely related populations in bimodal samples becomes possible.

## MATERIALS AND METHODS

**CdSe Nanoparticle Synthesis.** CdSe nanocrystals were synthesized in 1-octadecene (ODE) following an existing preparation.[54] All reactions utilized standard air-free techniques. Samples of 0.51 g of CdO (99.99%, Aldrich), 3.76 g of oleic acid (tech grade, Aldrich), and 160 mL of ODE (tech grade, 90%, Aldrich) were heated to 300 °C in a 500 mL three-neck flask. A selenium solution containing 0.16 g of Se powder (99.5%, Aldrich) dissolved in 0.8 g of trioctylphosphine (tech grade, 90%, Aldrich) and 5 mL of ODE was prepared and loaded into a syringe. When the solution of CdO became optically clear, the selenium solution was quickly injected. The reaction was halted by the rapid addition of 70 mL of room-temperature ODE at varying reaction times. Aliquots (~2 mL) of the reaction product were purified by adding an equal volume of acetone to precipitate waxy cadmium oleate, a reaction precursor. The samples were centrifuged for 10 min at 3200 rpm, and the colored decantate was collected. Excess acetone (99.6%, Fischer) was added to the decantate to precipitate the particles, and the solution was then centrifuged at 10 min and 3200 rpm to fully precipitate all nanocrystals. The precipitate was redissolved in the desired amount of toluene (99.8%, Fischer) and treated with ~30 μL of 1-dodecanethiol (98%, Aldrich) to provide a surface completely terminated by dodecanethiol.[50]

**$Fe_3O_4$ Nanoparticle Synthesis.** Ferroxyhydrate (γ-FeOOH, 30–50 mesh, Aldrich) was purchased and ground in a mortar to make a fine powder. In an airless solvothermal heating system, powdered iron oxide was dissolved in oleic acid (tech grade, Aldrich), diluted with 1-octadecene, and refluxed for 60 min. The black slurry was further purified by an acetone−hexane biphasic solvent system in a manner similar to that described above. $Fe_3O_4$ nanocrystals were isolated in stable hexane dispersions. Under these conditions, oleic acid is coordinated to the surface for stabilization. Further information about this synthetic method can be found elsewhere.[55]

**Synthesis of Au Nanoparticles.** Oleylamine-stabilized Au nanoparticles were synthesized following an existing preparation.[56] First, 0.112 g of $HAuCl_4 \cdot 3H_2O$ (>99%, Aldrich) was dissolved in 25 mL of deionized water in a 250 mL Erlenmeyer flask. Next, 0.365 g of tetraoctylammonium bromide (>99%, Fluka) dissolved in 25 mL of toluene (99.8%, Fischer) was added to the Au salt, resulting in a two-phase mixture. The mixture was stirred to transfer all color to the upper toluene layer. To the stirring mixture was added 0.829 g of oleylamine (70%, Aldrich) in 25 mL of toluene, resulting in white cloudiness. Finally, 0.165 g of $NaBH_4$ (99%, Aldrich) in 25 mL of deionized water was added, resulting in a clear brownish organic phase. The solution was allowed to stir for an additional 12 h. After 12 h, the organic phase was separated and then reduced to 5 mL using a Büchi R-200 rotary evaporator. The nanoparticles were precipitated with 250 mL of ethanol (190 proof, Aaper) and left in the freezer for 24 h at −10 °C. Once fully precipitated, the nanocrystals were collected by vacuum filtration and rinsed with more ethanol. These nanocrystals were redissolved in 100 mL of toluene and stored in a dark glass bottle in a refrigerator.

Gold nanocrystals were coated with thiol-terminated linear polystyrene by a grafting-to approach utilizing the strong affinity of thiols for gold. Four different samples were synthesized with polystyrene of varying molecular weights ($M_w$ = 1230, 2700, 5800, and 7700, Polymer Source Inc.). For each sample, $2.28 \times 10^{-3}$ g of the desired polymer was added to 100 μL of the as-prepared gold nanocrystals.

**Transmission Electron Microscopy and Particle Sizing.** A 100 kV JEOL transmission electron microscopy, model JEM-2010, was used to gather all images. Nanocrystals were drop-cast from their respective solvents onto carbon/Formvar-coated 300 mesh copper grids (Ted Pella no. 01821). Over 1000 nanocrystals were sized by hand for each sample using the ImagePro software suite, and the error introduced by population sampling from this analysis is <3% on average.[57] A larger issue is the difficulty in defining the edge of the particles; the objective focus at the time of image collection, as well as the contrast of the digital image, can lead to errors. We estimate these to be at most 3 Å. Our reported error bars on particle size take into account both of these sources of error in the measurement of the core diameter.

**Analytical Ultracentrifugation.** All experiments were run on a Beckman Optima XL-A ultracentrifuge with an AnTi-60 rotor equipped with absorbance optics. Sedimentation velocity experiments were run using double-sector aluminum centerpieces. The temperature was kept at 25 °C with an accuracy of 1 °C. At least 100 scans were taken for all experiments. Cadmium selenide and polystyrene-coated gold samples were run in tolu-

ene, and iron oxide samples were run in hexanes. Reported sedimentation coefficients are based on multiple run determinations for all samples, excluding the polystyrene-coated gold and 6 nm $Fe_3O_4$. Data analysis was performed using Ultrascan 7.1,[58] with the enhanced van Holde−Weischet analysis. The van Holde−Weischet analysis is a method that deconvolutes diffusion from sedimentation processes by extrapolation to infinite time. Briefly, each scan is divided into equal parts or fractions, and the radius value at each division is used in eq 1 to obtain the apparent sedimentation coefficients. Since each scan corresponds to a time, and a plot of the apparent sedimentation coefficients *versus* time$^{-0.5}$ can then be constructed. Lines of best fit are drawn through points from each division and extrapolated to the *y*-intercept, which corresponds to infinity. Intersection of all lines at a single point on the *y*-intercept indicates a uniform sample, while a broadly distributed sample has lines that intersect at multiple points. The fractions associated with each line and the sedimentation coefficient ($s_a$) at the point of intersection are combined into integral plots by graphing the integrated frequency *versus* the $s_a$. This integral distribution plot forms a perfectly vertical line for a uniform sample. Alternatively, the data can also be converted into a histogram or distribution plot by binning the sedimentation coefficients and calculating their frequency.[59,60] We also used SEDFIT and applied the ls-g(s*) analysis as a test case for our samples. We found the results to be within the range of experimental error, with the only difference being the width and shape of the *s*-value distribution. Additionally, we used SEDFIT to take into account solvent compressibility and found that the *s*-value varies within 10% of the actual values, in agreement with other observations.[61]

For the quantitative analysis presented in this work, the viscosity and density of the solvents are essential input parameters. The AU sample chamber is temperature controlled to within one degree. For the hexanes, the solvent for the iron oxide nanocrystals, we used a viscosity of 0.300 mPa and a density of 0.6603 g/cm$^3$ for the models shown in Figure 3. Toluene is the solvent for the cadmium selenide systems, and at 25 °C its viscosity is 0.560 mPa and its density is 0.8669 g/cm$^3$ The bulk densities for iron oxide, cadmium selenide, and gold were taken to be 5.17, 5.81, and 19.3 g/cm$^3$, respectively.[62] In order to correct for the size-dependent contribution to the density from the surface coating, we estimated the thicknesses of the oleic acid (iron oxide) and dodecanethiol (cadmium selenide) to be 2.0 and 1.2 nm, respectively.[50,63] The density of the surface coatings was assumed to be close to that of polystyrene, 1.12 g/cm$^3$.[62]

*Acknowledgment.* We thank Dr. Borries Demeler and Dr. Susan Cates for help with data analysis and helpful discussions. J.A.J. was supported by a training fellowship from the W.M. Keck Foundation to the Gulf Coast Consortia (NIH Grants 1 T90 DK70121-01 and 1 R90 DK71504-01). This work is supported by the Nanoscale Science and Engineering Initiative of the National Science Foundation under NSF Award No. EEC-0647452.

*Supporting Information Available:* Size-dependent sedimentation coefficients of iron oxide nanocrystals plotted against size for varying densities of the surface coating, TEM images and histograms of all nanocrystal samples, and a table of $s_a$ values, errors, and core sizes. This material is available free of charge *via* the Internet at http://pubs.acs.org.

## REFERENCES AND NOTES

1. Hiemenz, P. C.; Rajagopalan, R. Sedimentation and Diffusion and Their Equilibrium. In *Principles of Colloid and Surface Chemistry*, 3rd ed.; Marcel Dekker, Inc.: New York, 1997; pp 62–104..
2. Luccardini, C.; Tribet, C.; Vial, F.; Marchi-Artzner, V.; Dahan, M. Size, Charge, and Interactions with Giant Lipid Vesicles of Quantum Dots Coated with an Amphiphilic Macromolecule. *Langmuir* **2006**, *22*, 2304–2310.
3. Wang, X. Q.; Itoh, H.; Naka, K.; Chujo, Y. Tetrathiafulvalene-Assisted Formation of Silver Dendritic Nanostructures in Acetonitrile. *Langmuir* **2003**, *19*, 6242–6246.
4. Fei, B.; Lu, H. F.; Hu, Z. G.; Xin, J. H. Solubilization, Purification and Functionalization of Carbon Nanotubes Using Polyoxometalate. *Nanotechnology* **2006**, *17*, 1589–1593.
5. Jia, H. B.; Lian, Y. F.; Ishitsuka, M. O.; Nakahodo, T.; Maeda, Y.; Tsuchiya, T.; Wakahara, T.; Akasaka, T. Centrifugal Purification of Chemically Modified Single-Walled Carbon Nanotubes. *Sci. Technol. Adv. Mater.* **2005**, *6*, 571–581.
6. Maeda, Y.; Kanda, M.; Hashimoto, M.; Hasegawa, T.; Kimura, S.; Lian, Y.; Wakahara, T.; Akasaka, T.; Kazaoui, S.; Minami, N.; *et al.* Dispersion and Separation of Small-Diameter Single-Walled Carbon Nanotubes. *J. Am. Chem. Soc.* **2006**, *128*, 12239–12242.
7. Maeda, Y.; Kimura, S.-i.; Kanda, M.; Hirashima, Y.; Hasegawa, T.; Wakahara, T.; Lian, Y.; Nakahodo, T.; Tsuchiya, T.; Akasaka, T.; *et al.* Large-Scale Separation of Metallic and Semiconducting Single-Walled Carbon Nanotubes. *J. Am. Chem. Soc.* **2005**, *127*, 10287–10290.
8. Yu, A. P.; Bekyarova, E.; Itkis, M. E.; Fakhrutdinov, D.; Webster, R.; Haddon, R. C. Application of Centrifugation to the Large-Scale Purification of Electric Arc-Produced Single-Walled Carbon Nanotubes. *J. Am. Chem. Soc.* **2006**, *128*, 9902–9908.
9. Lu, Q.; Keskar, G.; Ciocan, R.; Rao, R.; Mathur, R. B.; Rao, A. M.; Larcom, L. L. Determination of Carbon Nanotube Density by Gradient Sedimentation. *J. Phys. Chem. B* **2006**, *110*, 24371–24376.
10. Chen, Z. H.; Du, X.; Du, M. H.; Rancken, C. D.; Cheng, H. P.; Rinzler, A. G. Bulk Separative Enrichment in Metallic or Semiconducting Single-Walled Carbon Nanotubes. *Nano Lett.* **2003**, *3*, 1245–1249.
11. Remsen, E. E.; Thurmond, K. B., II; Wooley, K. L. Solution and Surface Charge Properties of Shell Cross-Linked Knedel Nanoparticles. *Macromolecules* **1999**, *32*, 3685–3689.
12. Tziatos, C.; Precup, A. A.; Weidl, C. H.; Schubert, U. S.; Schuck, P.; Durchschlag, H.; Machtle, W.; van den Broek, J. A.; Schubert, D. Studies on the Partial Specific Volume of a Poly(Ethylene Glycol) Derivative in Different Solvent Systems. *Prog. Colloid Polym. Sci.* **2002**, *119*, 24–30.
13. Alley, S. C.; Trakselis, M. A.; Mayer, M. U.; Ishmael, F. T.; Jones, A. D.; Benkovic, S. J. Building a Replisome Solution Structure by Elucidation of Protein-Protein Interactions in the Bacteriophage T4 DNA Polymerise Holoenzyme. *J. Biol. Chem.* **2001**, *276*, 39340–39349.
14. Fernando, A. N.; Furtado, P. B.; Clark, S. J.; Gilbert, H. E.; Day, A. J.; Sim, R. B.; Perkins, S. J. Associative and Structural Properties of the Region of Complement Factor H Encompassing the Tyr402his Disease-Related Polymorphism and Its Interactions with Heparin. *J. Mol. Biol.* **2007**, *368*, 564–581.
15. Scott, D. J.; Harding, S. E.; Rowe, A. J. *Analytical Ultracentrifugation: Techniques and Methods*; Royal Society of Chemistry: London, 2006.
16. Laue, T. M.; Stafford, W. F., III. Modern Applications of Analytical Ultracentrifugation. *Annu. Rev. Biophys. Biomol. Struct.* **1999**, *28*, 75–100.
17. Machtle, W.; Borger, L. *Analytical Ultracentrifugation of Polymers and Nanoparticles*, 1st ed.; Springer: Berlin, 2006.
18. Leibowitz, J.; Lewis, M. S.; Schuck, P. Modern Analytical Ultracentrifugation in Protein Science: A Tutorial Review. *Protein Sci.* **2002**, *11*, 2067–2079.
19. Lechner, M. D.; Machtle, W. Characterization of Nanoparticles. In *Trends in Advanced Materials and Processes*; Trans Tech Publications Ltd.: Zurich-Uetikon, 2000; Vol. *352*, pp 87–90..
20. Wohlgemuth, M.; Machtle, W.; Mayer, C. Improved Preparation and Physical Studies of Polybutylcyanoacrylate Nanocapsules. *J. Microencapsul.* **2000**, *17*, 437–448.
21. Lechner, M. D.; Machtle, W. Characterization of Nanoparticles. *Macromol. Symp.* **1999**, *145*, 1–7.
22. Rager, T.; Meyer, W. H.; Wegner, G.; Mathauer, K.; Machtle, W.; Schrof, W.; Urban, D. Block Copolymer Micelles as Seed in Emulsion Polymerization. *Macromol. Chem. Phys.* **1999**, *200*, 1681–1691.

23. Kehrhahn, J. H.; Lechner, M. D.; Machtle, W. Analytical Ultracentrifugation with the New Optima Xl-a and Its Digital Uv/Vis Detector—Determination of Molar-Mass Distribution of Polymers from Sedimentation-Velocity. *Polymer* **1993**, *34*, 2447–2452.
24. Bronstein, L. M.; Khotina, I. A.; Chernyshov, D. M.; Valetsky, P. M.; Timofeeva, G. I.; Dubrovina, L. V.; Stein, B.; Karlinsey, R.; Triolo, A.; Weidenmann, A.; *et al. J. Colloid Interface Sci.* **2006**, *299*, 944–952.
25. Colfen, H.; Volkel, A.; Shinichi, E.; Kobold, U.; Kaufmann, J.; Puhlmann, A.; Goltner, C.; Wachernig, H. Mechanism of Nanoparticle-Enhanced Turbidimetric Assays Applying Nanoparticles of Different Size and Immunoreactivity. *Langmuir* **2002**, *18*, 7623–7628.
26. Colfen, H. Analytical Ultracentrifugation of Nanoparticles. *Polym. News* **2004**, *29*, 101–116.
27. Gohon, Y.; Giusti, F.; Prata, C.; Charvolin, D.; Timmins, P.; Ebel, C.; Tribet, C.; Popot, J. L. Well-Defined Nanoparticles Formed by Hydrophobic Assembly of a Short and Polydisperse Random Terpolymer, Amphipol A8−35. *Langmuir* **2006**, *22*, 1281–1290.
28. Joralemon, M. J.; Murthy, K. S.; Remsen, E. E.; Becker, M. L.; Wooley, K. L. Synthesis, Characterization, and Bioavailability of Mannosylated Shell Cross-Linked Nanoparticles. *Biomacromolecules* **2004**, *5*, 903–913.
29. Vogel, V.; Gohy, J.-F.; Lohnmeijer, B. G. G.; van der Broek, J. A.; Haase, W.; Schubert, U. S.; Schubert, D. Metallo-Supramolecular Micelles: Studies by Analytical Ultracentrifugation and Electron Microscopy. *J. Polym. Sci. A: Polym. Chem.* **2003**, *41*, 3159–3168.
30. Edelstein, S. J.; Schachman, H. K. The Simultaneous Determination of Partial Specific Volumes and Molecular Weights with Microgram Quantities. *J. Biol. Chem.* **1967**, *242*, 306–311.
31. Colfen, H.; Tirosh, S.; Zaban, A. Nanocrystal Surface Structure Analysis by Analytical Ultracentrifugation. *Langmuir* **2003**, *19*, 10654–10659.
32. Niederberger, M.; Garnweiter, G.; Krumeich, F.; Nesper, R.; Colfen, H.; Antonietti, M. Tailoring the Surface and Solubility Properties of Nanocrystalline Titania by a Nonaqueous in Situ Functionalization Process. *Chem. Mater.* **2004**, *16*, 1202–1208.
33. Nichols, J. B.; Kraemer, E. O.; Bailey, E. D. The Particle Size and Constitution of Colloidal Ferric Oxide. *J. Phys. Chem.* **1932**, *36*, 326–339.
34. Pinna, N.; Grancharov, S.; Beato, P.; Bonville, P.; Antonietti, M.; Niederberger, M. Magnetite Nanocrystals: Nonaqueous Synthesis, Characterization, and Solubility. *Chem. Mater.* **2005**, *17*, 3044–3049.
35. Borger, L.; Colfen, H.; Antonietti, M. Synthetic Boundary Crystallization Ultracentrifugation: A New Method for the Observation of Nucleation and Growth of Inorganic Colloids and the Determination of Stabilizer Efficiencies. *Colloids Surf. A: Physicochem. Eng. Aspects* **2000**, *163*, 29–38.
36. Dollefeld, H.; Hoppe, K.; Kolny, J.; Schilling, K.; Weller, H.; Eychmuller, A. Investigations on the Stability of Thiol Stabilized Semiconductor Nanoparticles. *Phys. Chem. Chem. Phys.* **2002**, *4*, 4747–4753.
37. Robinson, B. H.; Towey, T. F.; Zourab, S.; Visser, A. J. W. G.; van Hock, A. Characterisation of Cadmium Sulphide Colloids in Reverse Micelles. *Colloids Surf.* **1991**, *61*, 175–188.
38. Colfen, H.; Schnablegger, H.; Fisher, A.; Jentoft, F. C.; Weinberg, G.; Schlogl, R. Particle Growth Kinetics in Zirconium Sulfate Aqueous Solutions Followed by Dynamic Light Scattering and Analytical Ultracentrifugation: Implications for Thin Film Deposition. *Langmuir* **2002**, *18*, 3500–3509.
39. Svedberg, E. B.; Ahner, J.; Sukla, N.; Ehrman, S. H.; Schilling, K. Fept Nanoparticle Hydrodynamic Size and Densities Form the Polyol Process as Determined by Analytical Ultracentrifugation. *Nanotechnology* **2005**, *16*, 953–956.
40. Colfen, H. Analysis of Nanoparticles <10nm by Analytical Ultracentrifugation. *ACS Symp. Ser.* **2004**, *881*, 119–137.
41. Deshpande, A. S.; Pinna, N.; Beato, P.; Antonietti, M.; Niederberger, M. Synthesis and Characterization of Stable and Crystalline $Ce_{1-x}Zr_xO_2$ Nanoparticle Sols. *Chem. Mater.* **2004**, *16*, 2599–2604.
42. Koetz, J.; Bahnemann, J.; Lucas, G.; Tiersch, B.; Kosmella, S. Polyelectrolyte-Modified Microemulsions as New Templates for the Formationof Nanoparticles. *Colloids Surf. A: Physicochem. Eng. Aspects* **2004**, *250*, 423–430.
43. Wang, T.; Colfen, H.; Antonietti, M. Nonclassical Crystallization: Mesocrystals and Morphology Change of Caco3 Crystals in the Presence of a Polyelectrolyte Additive. *J. Am. Chem. Soc.* **2005**, *127*, 3246–3247.
44. Colfen, H.; Pauck, T. Determination of Particle Size Distributions with Angstrom Resolution. *Polym. Sci.* **1997**, *275*, 175–180.
45. Bronstein, L.; Sidorov, S. N.; Valetsky, P. M.; Hartmann, J.; Colfen, H.; Antonietti, M. Induced Micellization by Interaction of Poly(2-vinylpyridine)-*block*-poly(ethylene oxide) with Metal Compounds. Micelle Characteristics and Metal Nanoparticle Formation. *Langmuir* **1999**, *15*, 6256–6262.
46. Bronstein, L.; Chernyshov, D. M.; Timofeeva, G. I.; Dubrovina, L. V.; Valetsky, P. M.; Obolonkova, E. S.; Khokhlov, A. R. Interaction of Polystyrene-*block*-poly(ethylene oxide) Micelles with Cationic Surfactant in Aqueous Solutions. Metal Colloid Formation in Hybrid Systems. *Langmuir* **2000**, *16*, 3626–3632.
47. Calabretta, M.; Jamison, J. A.; Falkner, J. C.; Liu, Y.; Yuhas, B. D.; Matthews, K. S.; Colvin, V. L. Analytical Ultracentrifugation for Characterizing Nanocrystals and Their Bioconjugates. *Nano Lett.* **2005**, *5*, 963–967.
48. Svedberg, T.; Nichols, J. B. Determination of Size and Distribution of Size of Particles by Centrifugal Methods. *J. Am. Chem. Soc.* **1923**, *45*, 2910–2917.
49. Schuck, P. Size-Distribution Analysis of Macromolecules by Sedimentation Velocity Ultracentrifugation and Lamm Equation Modeling. *Biophys. J.* **2000**, *78*, 1606–1619.
50. Krueger, K. M.; Al-Somali, A. M.; Falkner, J. C.; Colvin, V. L. Characterization of Nanocrystalline Cdse by Size Exclusion Chromatography. *Anal. Chem.* **2005**, *77*, 3511–3515.
51. Yavuz, C. T.; Mayo, J. T.; Yu, W. W.; Prakash, A.; Falkner, J. C.; Yean, S.; Cong, L. L.; Shipley, H. J.; Kan, A.; Tomson, M.; *et al.* Low-Field Magnetic Separation of Monodisperse $Fe_3O_4$ Nanocrystals. *Science* **2006**, *314*, 964–967.
52. Lechner, M. D.; Machtle, W. Determination of the Particle Size Distribution of 5–100 nm Nanoparticles with the Analytical Ultracentrifuge: Consideration and Correction of Diffusion Effects. *Prog. Colloid Polym. Sci.* **1999**, *113*, 37–43.
53. Machtle, W. High-Resolution, Submicron Particle Size Distribution Analysis Using Gravitational-Sweep Sedimentation. *Biophys. J.* **1999**, *76*, 1080–1091.
54. Yu, W. W.; Peng, X. G. Formation of High-Quality Cds and Other II-VI Semiconductor Nanocrystals in Noncoordinating Solvents: Tunable Reactivity of Monomers. *Angew. Chem.* **2002**, *41*, 2368–2371.
55. Yu, W. W.; Falkner, J. C.; Yavuz, C. T.; Colvin, V. L. Synthesis of Monodisperse Iron Oxide Nanocrystals by Thermal Decomposition of Iron Carboxylate Salts. *Chem. Commun.* **2004**, 2306–2307.
56. Leff, D. V.; Brandt, L.; Heath, J. R. Synthesis and Characterization of Hydrophobic, Organically-Soluble Gold Nanocrystals Functionalized with Primary Amines. *Langmuir* **1996**, *12*, 4723–4730.
57. Vigneau, E.; Loisel, C.; Devaux, M. F.; Cantoni, P. Number of Particles for the Determination of Size Distribution from Microscopic Images. *Powder Technol.* **2000**, *107*, 243–250.
58. Demeler, B. Ultrascan: a Comprehensive Data Analysis Software Package for Analytical Ultracentrifugation Experiments. In *Modern Analytical Ultracentrifugation: Techniques and Methods*; Scott, D. J., Harding, S. E., Rowe, A. J., Eds.; Royal Society of Chemistry: London, 2005; pp 210–229.
59. Demeler, B.; Saber, H.; Hansen, J. C. Identification and Interpretation of Complexity in Sedimentation Velocity Boundaries. *Biophys. J.* **1997**, *72*, 397–407.

60. van Holde, K. E.; Weischet, W. O. Boundary Analysis of Sedimentation Velocity Experiments with Monodisperse and Paucidisperse Solutes. *Biopolymers* **1978**, *17*, 1387–1403.
61. Schuck, P. A Model for Sedimentation in Inhomogeneous Media. II. Compressibility of Aqueous and Organic Solvents. *Biophys. Chem.* **2004**, *108*, 187–200.
62. *CRC Handbook of Chemistry and Physics*, 87th ed.; Lide, D., Ed.; CRC Press: Boca Raton, FL, 2006–2007.
63. Zhang, Y. W.; Sun, X.; Si, R.; You, L. P.; Yan, C. H. Single-Crystalline and Monodisperse $LaF_3$ Triangular Nanoplates from a Single-Source Precursor. *J. Am. Chem. Soc.* **2005**, *127*, 3260–3261.